Available online at www.sciencedirect.com
SCIENCE DIRECT®
Journal of Power Sources 133 (2004) 277–285
JOURNAL OF POWER SOURCES
www.elsevier.com/locate/jpowsour

Mathematic simulation on power generation by roll cake type of thermoelectric double cylinders

Ryosuke O. Suzuki*

Department of Energy Science and Technology, Kyoto University, Yoshida-Honmachi, Sakyo-ku, Kyoto 606-8501, Japan

Received 24 October 2003; received in revised form 4 February 2004; accepted 10 February 2004

Available online 26 April 2004

Abstract

Analytical expression of electric power was deduced in case of the large-scale thermoelectric device that consists of the cylindrical double tubes like roll cake and is exposed to the two thermal fluids. The output powers of 16 systems were mathematically described by the simultaneous equations based on heat exchange. The temperature profiles in the device depend on the flow directions of hot and cold fluids, but the flow directions did not change the output power. Resultantly, eight sets of solutions for the output power were deduced. The maximum output power was the largest in the two systems (V2CC-I and V2CC-II system), where two fluids flow in counter directions and one of the fluids goes into the system from the inside of the inner cylinder. These chosen systems can generate the thermoelectric power equivalent with the single cylinder system (V1C system) using only 36% material of V1C.

Keywords: Thermoelectric generation; Thermoelectric device; Heat transfer; Thermal fluid; Bismuth telluride

1. Introduction

Thermal energy can be converted directly to the electricity in a thermoelectric power plant, where the thermoelectric motive force (EMF) due to Seebeck effect is generated proportional to a temperature difference $\Delta\theta$ between the hot and cold junctions. The larger $\Delta\theta$ to all the thermoelectric panels is generally given by the fluids, which carry the heat from the isolated sources. The hot fluid warms the hot junctions from the surface of thermoelectric modules, and the cold fluid cools the other junctions in the same way. Therefore, the heat is transmitted to the cold fluid through the thermoelectric materials. Basing on the heat exchange, the previous studies reported that the maximum of output power exists corresponding to a certain module size [1–10]. This is because the more serial connections of thermoelements can generate the higher voltage, but because the output power decreases both by the higher electrical resistance and by the smaller $\Delta\theta$ due to the larger heat exchange through the modules.

When the thermoelectric panels are connected three-dimensionally [6–10], the dimension of the thermoelectric device can be shortened. For example, the flat panels stacked multiply could save the space for the power generation; the same power could be generated in the four-panel-system by 22.5% space of the single panel [7,8].

The form of cylindrical tubes is more suitable for fluid circulation. The multiple tube (T) systems were reported previously [6,8]. Alternatively, the vortical (V) cylindrical system as shown in Fig. 1 circulates the fluids vortically in the gaps between the thermoelectric panels. This V system can flow the larger amount of fluid with the less pressure loss than T systems, and it has the potential to produce a large power. Fig. 1(a) looks like roll cake and consists of the double thermoelectric cylinders, among which a hot fluid and a cold fluid flow as counter flow.

The mathematical expression of its output power was previously reported in the three models simplified as Fig. 1(b)–(d), and the double cylinder system with counter flow (V2CC system, Fig. 1(d)) was enough efficient for miniaturization, comparing with the single cylinder (V1) systems [10]. However, the other possible flow directions, as shown in Fig. 2(b)–(p), may hold the same potential, although they were not analyzed. For the practical operation of the thermoelectric power generation with the multiple cylinders, the choice of fluid directions should be clarified from the fundamental bases.

Mode I and II in Fig. 2 show a pair of alternative selection of the fluid path whether the hot fluid flows between two thermoelectric cylinders or outside them. Mode I and II show

* Tel.: +81-75-753-5453; fax: +81-75-753-5432.
E-mail address: suzuki@energy.kyoto-u.ac.jp (R.O. Suzuki).

0378-7753/$ – see front matter © 2004 Elsevier B.V. All rights reserved.
doi:10.1016/j.jpowsour.2004.02.014

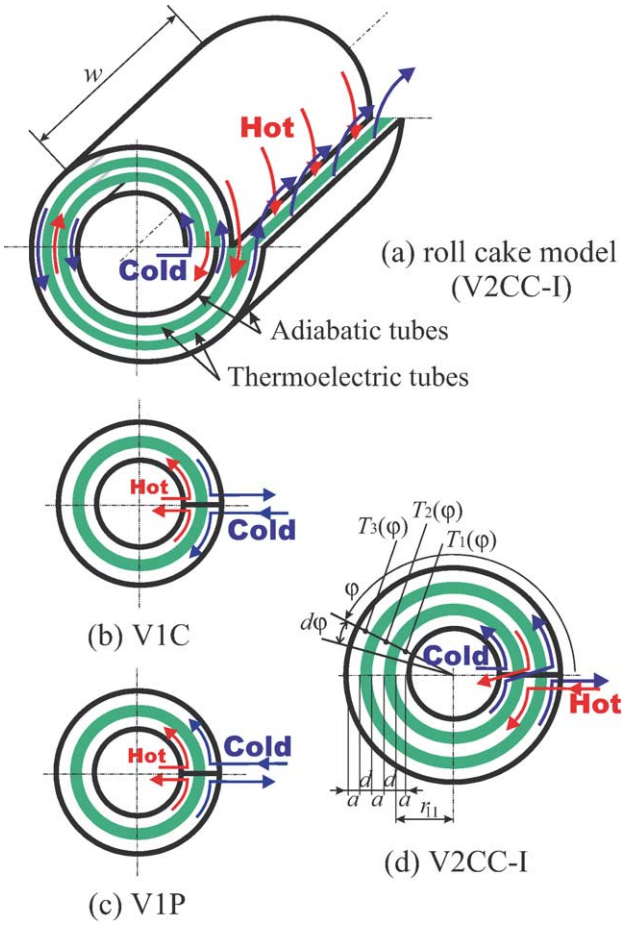

Fig. 1. Vortical systems with the cylindrical thermoelectric tubes.

the cases that the fresh fluid enters from the inside of the cylinder, while it enters from the outside in Mode III and IV. In Mode I and III, a hot fluid is sandwiched by two cold fluids, while a cold fluid is sandwiched by two hot fluids in Mode II and IV.

The purpose of this work is to deduce the mathematical expressions of the thermoelectric power extractable from the double cylinder systems (Fig. 2), and to search for the further improvements in the operation. The choices of flow directions and fluid paths suitable for high output are focused.

2. Basic assumptions and models

A brief outline of the methods for modeling and mathematical analysis will be given here because their details of the common bases were reported separately [6–10].

2.1. Directions and paths of fluids

For easy mathematical handling, the roll cake systems (Fig. 1(a)) are simplified to the systems with the combined multi-cylinders (Fig. 2). Therefore, the vortical double systems (V2 systems) consist of two thermoelectric cylinders and three paths for fluids. The two fluids occupy these paths, and one of the fluids is circulated twice. The systems are classified by the direction of fluid flow (counter flow, "C", and parallel flow, "P") and the choice of fluid paths (Mode I–IV). For example, in the V2CC-I system, the cold fluid flows the most inner path (Mode I) and all the fluids in three paths flow in counter mode (first C for inner cylinder and second C for the outer cylinder). The hydrodynamic boundary conditions for 18 mathematical models are listed in Table 1.

2.2. Cylindrical thermoelectric tubes

Our thermoelectric module consists of cylindrical fan-shaped thermoelements with a single layer of Π-type p–n junctions, as shown in Fig. 3 [10]. All the thermoelements are homogeneously aligned and connected electrically in series. The hot and cold fluids flow along the both cylindrical surfaces in the direction of $\pm\varphi$ (see Fig. 1(d)). The temperature of the fluid j, $T_j(\varphi)$, becomes as a function of φ. The inhomogeneities such as fins, electrodes and isolators are neglected or considered as the heat transfer coefficient, h, of the smooth surface.

3. Equations for output power

3.1. Deduction of equations

Considering the angular dependency of $T_j(\varphi)$, the heat transfer coefficient K_i is first calculated as the over-all heat transfer coefficient per unit length through the cylinder i in the direction perpendicular to r axis [9–12]:

$$K_i = \frac{1}{(1/h_{i,i}r_{i,i}) + \ln(r_{i,i+1}/r_{i,i})/\lambda + 1/h_{i,i+1}r_{i,i+1}}. \quad (1)$$

where $r_{i,j}$ and $h_{i,j}$ are the radius of the cylinder and the heat transfer coefficient between the cylinder i and the fluid j, respectively. λ is the average heat conductivity of the module, defined by

$$\lambda = \frac{\lambda_p L_p + \lambda_n L_n}{L_p + L_n} = \frac{\lambda_p L_p + \lambda_n L_n}{L}, \quad (2)$$

where λ_p, λ_n, L_p and L_n are the heat conductivity and the length of p- and n-type elements, respectively. Fig. 3 shows the assumed setup of thermoelectric junctions. L is the unit size of a thermoelectric pair. Therefore, $L = L_p + L_n$.

Because our systems consist of two cylinders, a set of three simultaneous derivative equations is written from the heat transfers through two cylinders:

$$M_1 C_{p,1} \frac{dT_1(\varphi)}{d\varphi} = \pm K_1 w(T_1(\varphi) - T_2(\varphi)), \quad (3)$$

$$\pm M_2 C_{p,2} \frac{dT_2(\varphi)}{d\varphi} = \pm K_1 w(T_1(\varphi) - T_2(\varphi)) \pm K_2 w(T_2(\varphi) - T_3(\varphi)), \quad (4)$$

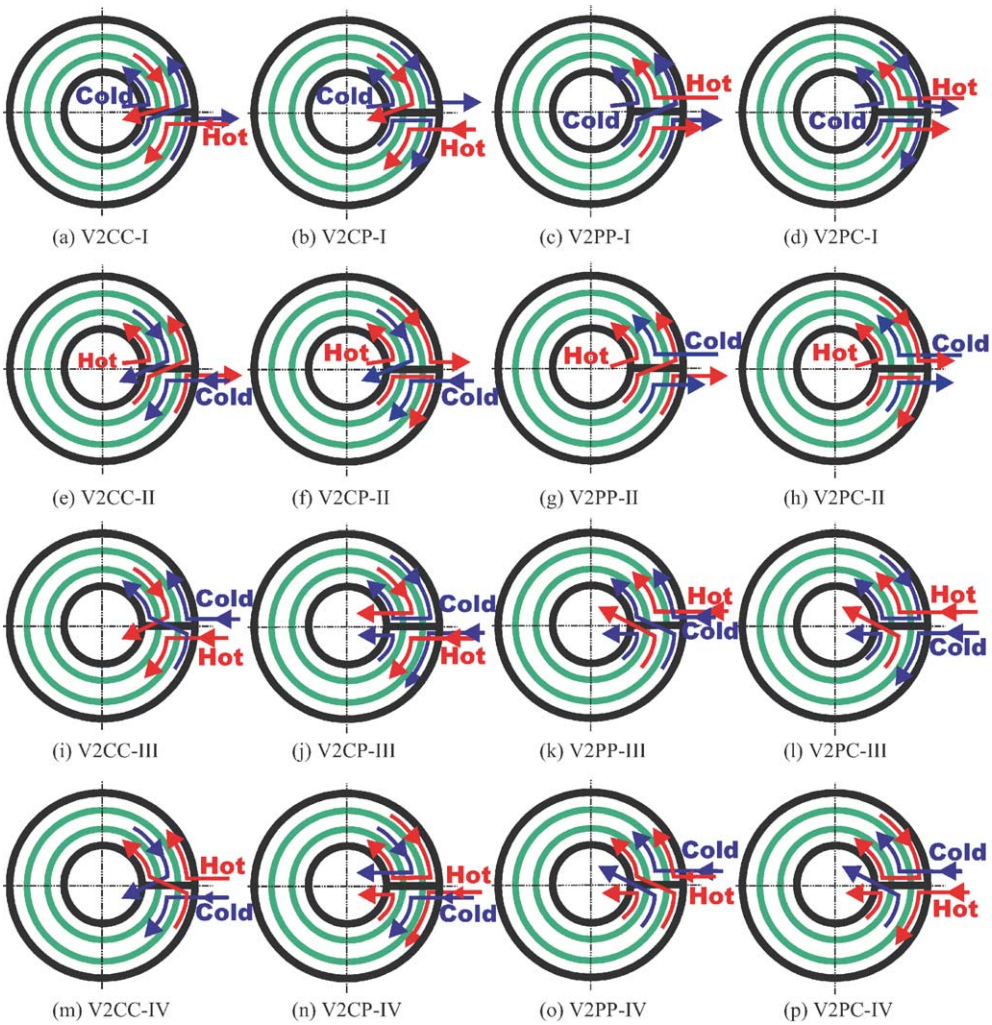

Fig. 2. Analyzed systems with the double cylindrical thermoelectric tubes.

$$\pm M_3 C_{p,3} \frac{\mathrm{d}T_3(\varphi)}{\mathrm{d}\varphi} = \pm K_2 w (T_2(\varphi) - T_3(\varphi)), \tag{5}$$

where M_i and $C_{p,i}$ are mass flow rate and heat capacity for fluid i, respectively. For simplicity, the steady state is considered, and the heat transfer by Peltier effect and the exothermal heat by Joule effect are neglected. The choice of sign '±' in Eqs. (3)–(5) depends on the system design. The temperature $\theta_{i,j}(\varphi)$ at the p–n junction in the cylinder i facing to the fluid j is written using $T_j(\varphi)$:

$$\theta_{i,i+1}(\varphi) - \theta_{i,i}(\varphi) = \frac{K_i}{\lambda}\{T_{i+1}(\varphi) - T_i(\varphi)\} \ln\left(\frac{r_{i,i+1}}{r_{i,i}}\right). \tag{6}$$

The electromotive force, E, is the summation of EMF over the two cylinders:

$$E = E_1 + E_2 = \sum_{i=1}^{2}\left[\frac{N_\phi n_x w \alpha}{2\pi}\int_0^{2\pi}\{\theta_{i,i}(\varphi) - \theta_{i+1,i}(\varphi)\}\,\mathrm{d}\varphi\right], \tag{7}$$

where α is the difference between the Seebeck coefficients of p and n elements, N_ϕ and n_x are the number of thermoelectric pairs along a cylindrical circulation, and the number density of pairs in the cylinder length direction, respectively. Therefore, $N_\phi = 2\pi/\phi$ and $n_x = 1/L$. ϕ is the circumferential angle of a pair. The electric resistance, R_i, is deduced

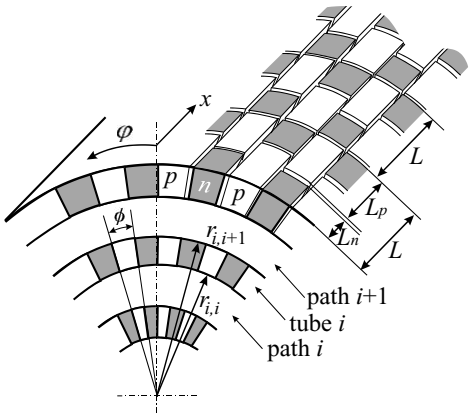

Fig. 3. Dimensions of thermoelectric modules.

Table 1
Conditions for the analyzed systems

System	Direction of fluids[a]	Boundary conditions	Model	Reference
V1C	$d_1 > 0$, $d_2 < 0$	$T_1(0) = T_h^{in}$, $T_2(2\pi) = T_c^{in}$	Fig. 1(b)	[10]
V1P	$d_1 > 0$, $d_2 > 0$	$T_1(0) = T_h^{in}$, $T_2(0) = T_c^{in}$	Fig. 1(c)	[10]
V2CC-I	$d_1 > 0$, $d_2 < 0$, $d_3 = d_1 > 0$	$T_1(0) = T_c^{in}$, $T_2(2\pi) = T_h^{in}$, $T_3(0) = T_1(2\pi)$	Figs. 1(d) and 2(a)	[10]
V2CC-II	ibid.	$T_1(0) = T_h^{in}$, $T_2(2\pi) = T_c^{in}$, $T_3(0) = T_1(2\pi)$	Fig. 2(e)	
V2CC-III	ibid.	$T_1(0) = T_3(2\pi)$, $T_2(2\pi) = T_h^{in}$, $T_3(0) = T_c^{in}$	Fig. 2(i)	
V2CC-IV	ibid.	$T_1(0) = T_3(2\pi)$, $T_2(2\pi) = T_c^{in}$, $T_3(0) = T_h^{in}$	Fig. 2(m)	
V2CP-I	$d_1 > 0$, $d_2 < 0$, $d_3 = -d_1 < 0$	$T_1(0) = T_c^{in}$, $T_2(2\pi) = T_h^{in}$, $T_3(2\pi) = T_1(2\pi)$	Fig. 2(b)	
V2CP-II	ibid.	$T_1(0) = T_h^{in}$, $T_2(2\pi) = T_c^{in}$, $T_3(2\pi) = T_1(2\pi)$	Fig. 2(f)	
V2CP-III	ibid.	$T_1(0) = T_3(0)$, $T_2(2\pi) = T_h^{in}$, $T_3(2\pi) = T_c^{in}$	Fig. 2(j)	
V2CP-IV	ibid.	$T_1(0) = T_3(0)$, $T_2(2\pi) = T_c^{in}$, $T_3(2\pi) = T_h^{in}$	Fig. 2(n)	
V2PP-I	$d_1 > 0$, $d_2 > 0$, $d_3 = d_1 > 0$	$T_1(0) = T_c^{in}$, $T_2(0) = T_h^{in}$, $T_3(0) = T_1(2\pi)$	Fig. 2(c)	
V2PP-II	ibid.	$T_1(0) = T_h^{in}$, $T_2(0) = T_c^{in}$, $T_3(0) = T_1(2\pi)$	Fig. 2(g)	
V2PP-III	ibid.	$T_1(0) = T_3(2\pi)$, $T_2(0) = T_h^{in}$, $T_3(0) = T_c^{in}$	Fig. 2(k)	
V2PP-IV	ibid.	$T_1(0) = T_3(2\pi)$, $T_2(0) = T_c^{in}$, $T_3(0) = T_h^{in}$	Fig. 2(o)	
V2PC-I	$d_1 > 0$, $d_2 > 0$, $d_3 = -d_1 < 0$	$T_1(0) = T_c^{in}$, $T_2(0) = T_h^{in}$, $T_3(2\pi) = T_1(2\pi)$	Fig. 2(d)	
V2PC-II	ibid.	$T_1(0) = T_h^{in}$, $T_2(0) = T_c^{in}$, $T_3(2\pi) = T_1(2\pi)$	Fig. 2(h)	
V2PC-III	ibid.	$T_1(0) = T_3(0)$, $T_2(0) = T_h^{in}$, $T_3(2\pi) = T_c^{in}$	Fig. 2(l)	
V2PC-IV	ibid.	$T_1(0) = T_3(0)$, $T_2(0) = T_c^{in}$, $T_3(2\pi) = T_h^{in}$	Fig. 2(p)	

[a] When the vector of fluid i is defined as $\vec{M}_i$ at $\varphi = 0$, $\vec{M}_i$ is written as $\vec{M}_i = d_i\vec{e}_i$, where $\vec{e}_i$ is an unit vector in the positive direction at $\varphi = 0$ and d_i is a constant. The mass flow rate, M_i, is equal to $|d_i|$.

by integrating the resistance of a thin fan-shaped layer in the direction of radius:

$$R_i = \frac{N_\varphi^2 n_x w}{2\pi}\left(\frac{\rho_p}{L_p} + \frac{\rho_n}{L_n}\right)\ln\left(\frac{r_{i,i+1}}{r_{i,i}}\right), \tag{8}$$

where ρ_p and ρ_n are the specific resistivity of p and n elements, respectively.

Finally, the output power, P, is optimized by balancing the internal and external resistances:

$$P = \frac{E^2}{4(R_1 + R_2)}. \tag{9}$$

This work uses hereafter this P, where the internal resistance is equal to the external resistance.

3.2. Equations of output power

The simultaneous equations Eqs. (3)–(5) could be analytically solved, but the explicit expression of the solutions, $T_j(\varphi)$, were complicated and the mathematical form of P became very long. The following conditions are used hereafter in order to express simply the analytical difference among the V2 systems:

$$|M_1 C_{p,1}| = |M_2 C_{p,2}| = |M_3 C_{p,3}| = MC_p. \tag{10}$$

The effect of MC_p on P was discussed for V1 systems [10].

Under these situations, the simultaneous equations Eqs. (3)–(5) can be re-written as

$$\frac{\mathrm{d}}{\mathrm{d}\varphi}\begin{pmatrix} T_1(\varphi) \\ T_2(\varphi) \\ T_3(\varphi) \end{pmatrix} = m\begin{pmatrix} T_1(\varphi) \\ T_2(\varphi) \\ T_3(\varphi) \end{pmatrix}. \tag{11}$$

where the matrix, m, depends on the system design as listed in Table 2.

Using the procedure mentioned above, the output power for the V2 systems was calculated and listed also in Table 2. The definitions of K_{a1}, K_{a2} and X are identical with the previous works [9,10]. The result for V2CC-I system agreed with the previous report [10]. The temperature dependencies of all the variables are neglected for simplification. Although they can affect the output power, the output power cannot be deduced in the analytical way if we consider the temperature dependencies of the materials' parameters. The numerical solution with such considerations will be reported separately.

First it is noted that the output powers of Mode I were equal to those of Mode II in four types of fluid direction. Similarly those of Mode III were equal to those of Mode IV. Namely, the path choice for the hot fluid did not affect the output power. Only a difference was the sign of EMF.

Second, the output power contained the common term of $A = n_x M^2 Cp^2 L_n L_p \alpha^2 (T_h^{in} - T_c^{in})^2/\lambda w(L_p\rho_n + L_n\rho_p)$. The output power was simply proportional to $n_x\alpha^2(T_h^{in} - T_c^{in})^2$. All the output powers were independent from the number of thermoelectric elements, N_ϕ. The contributions of the other variables are not simple because they affect through the other terms.

The other parts were the complicate functions of system geometry, material properties and overall heat transfer

Table 2
Matrix for the differential equation and the output power, where $M_1C_{p,1} = |M_2C_{p,2}| = |M_3C_{p,3}| = MC_p$

System	Matrix, m	Output power, P
V2CC-I and V2CC-II	$m = \begin{pmatrix} -f_1 & f_1 & 0 \\ -f_1 & f_1+f_2 & -f_2 \\ 0 & f_2 & -f_2 \end{pmatrix}$	$P = \frac{A}{2(Ka_1+Ka_2)}\left[\frac{\sinh(X)\{(K_1Ka_1+K_2Ka_2)\cosh(X)+\sqrt{K_1K_2}(Ka_1-Ka_2)\sinh(X)\}}{\sqrt{K_1K_2}\cosh(2X)+(K_1+K_2)\sinh(2X)}\right]^2$
V2CC-III and V2CC-IV	ibid.	$P = \frac{A}{2(Ka_1+Ka_2)}\left[\frac{\sinh(X)\{(K_1Ka_1+K_2Ka_2)\cosh(X)+\sqrt{K_1K_2}(-Ka_1+Ka_2)\sinh(X)\}}{\sqrt{K_1K_2}\cosh(2X)+(K_1+K_2)\sinh(2X)}\right]^2$
V2CP-I and V2CP-II	$m = \begin{pmatrix} -f_1 & f_1 & 0 \\ -f_1 & f_1+f_2 & -f_2 \\ 0 & -f_2 & f_2 \end{pmatrix}$	$P = \frac{A}{8(Ka_1+Ka_2)}\left[\frac{\sqrt{K_2}(Ka_1-Ka_2)\{\cosh(2Z)-F\}+\sqrt{K_1+K_2}Ka_1\sinh(2Z)}{\sqrt{K_2}\cosh(2Z)+\sqrt{K_1+K_2}\sinh(2Z)}\right]^2$
V2CP-III and V2CP-IV	ibid.	$P = \frac{A}{8(Ka_1+Ka_2)}\left[\frac{\sqrt{k_2}(Ka_1-Ka_2)(\cosh(2Z)-1/F)-\sqrt{K_1+K_2}Ka_1\sinh(2Z)}{\sqrt{K_2}\cosh(2Z)+\sqrt{K_1+K_2}\sinh(2Z)}\right]^2$
V2PP-I and V2PP-II	$m = \begin{pmatrix} -f_1 & f_1 & 0 \\ f_1 & -f_1-f_2 & f_2 \\ 0 & f_2 & -f_2 \end{pmatrix}$	$P = \frac{A}{8(Ka_1+Ka_2)}\left[\frac{MC_pU\{Ka_1\exp(-2V)-Ka_2\exp(2V)-(Ka_1-Ka_2)\cosh(2U)\}+\pi w(2K_1Ka_1-K_2Ka_1-K_1Ka_2+2K_2Ka_2)\sinh(2U)}{2U\exp(2V)+U\cosh(2U)+V\sinh(2U)}\right]^2$
V2PP-III and V2PP-IV	ibid.	$P = \frac{A}{8(Ka_1+Ka_2)}\left[\frac{MC_pU\{-Ka_1\exp(-2V)+Ka_2\exp(2V)+(Ka_1-Ka_2)\cosh(2U)\}+\pi w(2K_1Ka_1-K_2Ka_1-K_1Ka_2+2K_2Ka_2)\sinh(2U)}{2U\exp(2V)+U\cosh(2U)+V\sinh(2U)}\right]^2$
V2PC-I and V2PC-II	$m = \begin{pmatrix} -f_1 & f_1 & 0 \\ f_1 & -f_1-f_2 & f_2 \\ 0 & -f_2 & f_2 \end{pmatrix}$	$P = \frac{A}{8(Ka_1+Ka_2)}\left[\frac{\sqrt{K_1}(Ka_1-Ka_2)\{\cosh(2Y)-E\}+\sqrt{K_1+K_2}Ka_2\sinh(2Y)}{\sqrt{K_1}\cosh(2Y)+\sqrt{K_1+K_2}\sinh(2Y)}\right]^2$
V2PC-III and V2PC-IV	ibid.	$P = \frac{A}{8(Ka_1+Ka_2)}\left[\frac{\sqrt{K_1}(Ka_1-Ka_2)\{\cosh(2Y)-1/E\}-\sqrt{K_1+K_2}Ka_2\sinh(2Y)}{\sqrt{K_1}\cosh(2Y)+\sqrt{K_1+K_2}\sinh(2Y)}\right]^2$

Where $f_1 = K_1w/MC_p$, $f_2 = K_2w/MC_p$, $A = n_xM^2{C_p}^2L_nL_p\alpha^2(T_1^{in}-T_2^{in})^2/w\lambda(L_p\rho_n+L_n\rho_p)$, $E = \exp(-2\pi f_1)$, $F = \exp(2\pi f_2)$, $U = \pi\sqrt{{f_1}^2-f_1f_2+{f_2}^2}$, $V = \pi(f_1+f_2)$, $X = \pi\sqrt{f_1}\sqrt{f_2}$, $Y = \pi\sqrt{f_1(f_1+f_2)}$, $Z = \pi\sqrt{f_2(f_1+f_2)}$, $Ka_1 = (1/\pi\lambda)\ln(r_{12}/r_{11})$, and $Ka_2 = (1/\pi\lambda)\ln(r_{23}/r_{22})$.

coefficient K_i. Because K_i depended on the radius as written in Eqs. (1) and (2), our expressions could not be simplified analytically by the similar way with the flat multi-panels systems [7,8]. Therefore, the output power will be numerically compared using the thermo-physical values of Bi_2Te_3 semiconductors.

4. Numerical comparison of systems

4.1. Physical properties and module optimization

Table 3 shows a typical set of properties for an identical sample of the BiTe thermoelectric element at room temperature [13], and used for this work. Table 4 shows the fluid properties and the parameters for thermoelectric cylinders, considering the utilization of nitrogen gas. The heat transfer coefficient, h, was set to be independent of the flow rate and of the cross-section of fluid path. These values are identical with our previous studies [6–10].

The output power P in Table 2 was optimized against the geometrical factors, L_n and L_p, using that

$$L_n = \frac{\sqrt{\lambda_p \rho_n}}{\sqrt{\lambda_n \rho_p} + \sqrt{\lambda_p \rho_n}} L \quad \text{and} \quad L_p = \frac{\sqrt{\lambda_n \rho_p}}{\sqrt{\lambda_n \rho_p} + \sqrt{\lambda_p \rho_n}} L \tag{12}$$

Eq. (12) is generally taken for the analysis with the infinite heat sources, and it was also a good approximation for cylindrical geometry [9,10].

4.2. Maximum output power

Fig. 4 shows 18 kinds of the output power, which were thus optimized by Eq. (12) and calculated by the data given in Tables 3 and 4. Two solutions for V1 system are referred from [10]. The output powers of Mode I and III exactly agreed with those of Mode II and IV, respectively, naturally because the mathematical expressions are identical as shown in Table 2.

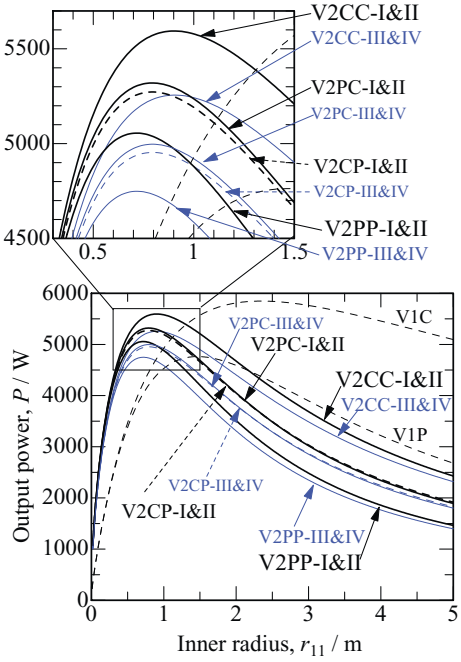

Fig. 4. Comparison of the output power of the systems, where the cylinder length $w = 2$ m.

As the inner radius, r_{11}, increased, the calculated output power increased to a maximum, P^{max}, at an optimized radius, $r_{11}^{opt.}$, and then decreased monotonically. This phenomenon was common for all systems, but P^{max} and $r_{11}^{opt.}$ were characteristic for the individual systems. It was difficult to deduce

Table 3
Specific values of thermoelectric elements used here

Materials	Seebeck coefficient, α (μV/K)	Resistivity, ρ (μΩ m)	Thermal conductivity, λ (W/K m)	Figure of merit, Z (K^{-1})
Bi–54.3 at.% Te (p)	162	5.55	2.06	2.605×10^{-3}
Bi–64.5 at.% Te (n)	−240	10.1	2.02	

Table 4
Parameters for thermoelectric power generation system

	Variables	Values used in this work
Thermoelectric device	Length, w	Variable (typically 2 m)
	Thickness of tube, d	Variable (typically 0.05 m)
	Inner radius of inner tube, r_{11}	Variable
	Distance between two tubes, a (fluid path height)	Variable (typically 0.1 m)
	Number density of pairs, n_x	50 m^{-1}
	Number of pairs round a circumferential cycle, N_ϕ	100
Thermal sources	Hot source	N_2 gas (inlet $T_h^{in} = 500$ K)
	Cold source	N_2 gas (inlet $T_c^{in} = 300$ K)
Gas properties	Specific heat, $C_{p,hot} = C_{p,cool}$	1044 J/kg K (at 400 K, 0.1 Pa)
	Mass flow rate, $M_{hot} = M_{cool}$	1.00 kg/s
	Heat transfer coefficient, $h_{1,1} = h_{1,2} = h_{2,2} = h_{2,3} = h_{hot} = h_{cool}$	500 W/m^2 K independent of flow rate

Table 5
Maximum output power, P^{max}, and thermoelectric motive force, $E^{opt.}$, at the optimized radius, $r_{11}^{opt.}$

System	Length of the tubes, w								
	1 m			2 m			5 m		
	P^{max} (W)	$E^{opt.}$ (V)	$r_{11}^{opt.}$ (m)	P^{max} (W)	$E^{opt.}$ (V)	$r_{11}^{opt.}$ (m)	P^{max} (W)	$E^{opt.}$ (V)	$r_{11}^{opt.}$ (m)
V2CC-I and V2CC-II	5531	375.6	1.880	5594	737.4	0.903	5703	1812	0.3345
V2CC-III and V2CC-IV	5361	362.2	1.883	5256	714.0	0.905	4881	1670	0.3375
V2CP-I and V2CP-II	5231	379.8	1.661	5273	759.3	0.793	5302	1845	0.2922
V2CP- III and V2CP-IV	5070	373.8	1.662	4954	735.1	0.795	4539	1702	0.2946
V2PP-I and V2PP-II	5010	389.5	1.504	5056	778.4	0.716	5084	1890	0.2611
V2PP- III and V2PP-IV	4855	383.3	1.505	4749	753.9	0.717	4349	1744	0.2627
V2PC-I and V2PC-II	5254	380.7	1.660	5320	762.7	0.793	5424	1870	0.2908
V2PC- III and V2PC-IV	5092	374.6	1.662	4997	738.3	0.795	4636	1725	0.2925

P^{max} and $r_{11}^{opt.}$ analytically, because they depended on heat transfer coefficient K_i in the complicated form. P^{max} and $r_{11}^{opt.}$ were numerically solved using the equations in Table 2, and they are listed in Table 5.

4.3. Temperature profiles

Figs. 5 and 6 show the temperature distributions when the cylinder radius was equal to the optimum inner radius, $r_{11}^{opt.}$. The surface temperatures, $\theta_{i,j}(\varphi)$, are shown in addition of the fluid temperatures, $T_j(\varphi)$. The hot and cold fluid are cooled and warmed, respectively, as they proceed along the module surface. The temperature profiles varied depending on the system design.

As shown in V2CC systems (Fig. 5), the temperature profiles for Mode I and II and for Mode III and IV were symmetric, and this causes the agreement of the output power in these modes. Therefore, the temperature profiles for the other systems were shown only for Mode I in Fig. 6.

As reported previously [10], the fluid temperatures of V1C system (Fig. 6) changed linearly when $M_1C_{p,1} = |M_2C_{p,2}|$, and the outlet temperatures of the hot and cold fluids were the same, 400 K ($T_{hot}^{out} = T_{cold}^{out} = (T_{hot}^{in} + T_{cold}^{in})/2$). However, the fluid temperatures of V2 systems were not linear. The hot fluid sandwiched by two cold fluids was cooled rapidly, and the temperature rises of coolants were slow. At the optimum conditions for P^{max}, the outlet temperatures of the hot and cold fluids (T_{hot}^{out} and T_{cold}^{out}) were above and below 400 K, respectively. It means that the thermal energy of the fluids in V2 systems did not exchanged so completely through the thermoelectric panels as that in V1 systems.

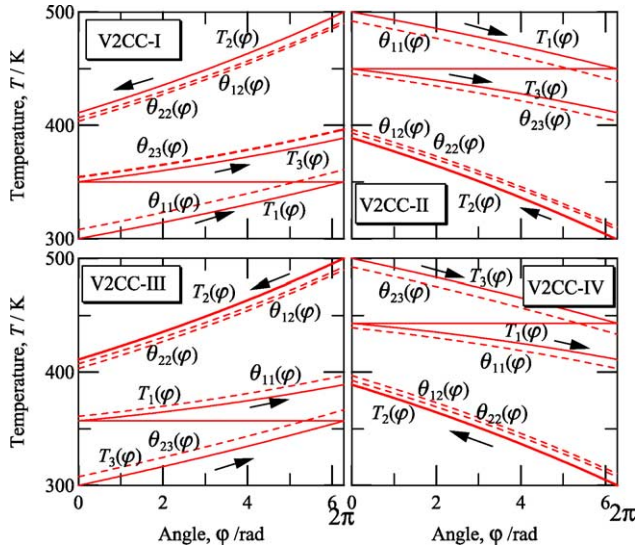

Fig. 5. Temperature profiles of V2CC system along the cylinder surfaces, when the output power becomes the maximum. The arrows show the fluid directions. T_1, T_2 and T_3 are temperatures of the fluids, and θ_{11}, θ_{12}, θ_{22} and θ_{23} are the surface temperatures ($w = 2$ m).

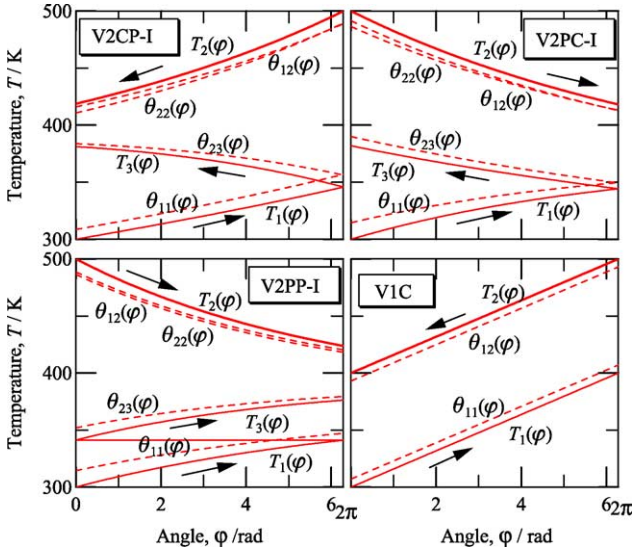

Fig. 6. Temperature profiles along the cylinder surfaces, when the output power becomes the maximum. The arrows show the fluid directions. T_1, T_2 and T_3 are temperatures of the fluids, and θ_{11}, θ_{12}, θ_{22} and θ_{23} are the surface temperatures ($w = 2$ m).

4.4. Largest P^{max}

The existence of P^{max} was reported also in the flat panels and the tubes [1–10]. It is partially because the larger thermoelectric panel size reduces the temperature difference ΔT between the two fluids.

As shown in Table 5 and Fig. 4, the maximum output power of V2CC-I and V2CC-II systems, P^{max}(V2CC-I and V2CC-II), was the largest, and P^{max}(V2PP-III and V2CC-IV) was the smallest in the V2 systems when the cylinder length w was fixed. However, $r_{11}^{opt.}$(V2CC-I and V2CC-II) was the largest and $r_{11}^{opt.}$(V2PP-III and V2CC-IV) was the smallest. This tendency consists with that for V1 systems [10]. The reason why P^{max}(counter flow) > P^{max}(parallel flow) can be qualitatively understood by the temperature profiles (Fig. 6) that $\sum \Delta T$(counter flow) is larger than $\sum \Delta T$(parallel flow) [7,11,12]. ΔT(V2CC) is nearly constant for all the thermoelectric elements, while ΔT(parallel flow) is large at the inlet but it decreases significantly. Therefore, the counter flow can generate larger power than the parallel flow, although the system size of counter flow to obtain the maximum output is larger than that of parallel flow [10].

It is noteworthy that P^{max}(V2CC-I and V2CC-II) was nearly equal to P^{max} in V1 systems, i.e., 98.7% of P^{max}(V1C) and 117.5% of P^{max}(V1P), when $w = 2$ m. However, $r_{11}^{opt.}$(V2CC-I and V2CC-II) was only 45.5% of $r_{11}^{opt.}$(V1C) and 61.6% of $r_{11}^{opt.}$(V1P). The amount of thermoelectric material necessary for P^{max}(V2CC-I and V2CC-II) is evaluated as 36.0 and 91.1% of those for P^{max}(V1C) and P^{max}(V1P), respectively. V2CC system is thus more compact and material saving than V1 systems.

The power difference between P^{max}(V2CC) and P^{max}(V2PP) was smaller than that between P^{max}(V1C) and P^{max}(V1P), and the radius difference between $r_{11}^{opt.}$(V2CC) and $r_{11}^{opt.}$(V2PP) was closer than that between $r_{11}^{opt.}$(V1C) and $r_{11}^{opt.}$(V1P). This means that the choice of flow directions in V2 systems was not so sensitive as in V1 systems to obtain the large output power.

4.5. V2CP and V2PC systems

The output power of V2CP-I and V2CP-II systems, P(V2CP-I and V2CP-II), was very close to P(V2PC-I and V2PC-II) in the wide range of radius, r_{11}, as shown in Fig. 4. Similarly P(V2CP-III and V2CP-IV), was very close to P(V2PC-III and V2PC-IV). The combination of counter and parallel flow may cancel their characters each other, and the output powers of V2CP and V2PC systems may become similar.

As illustrated in Fig. 2, these two systems need the sudden change of flow direction at $\varphi = 0$ or 2π. This causes the large pressure loss for fluid circulation. When we consider the realistic application in the V2 systems, therefore, the vortical continuous fluid flow such as Fig. 1(a) would be completed not by V2CP or V2PC systems, but by V2CC or V2PP systems.

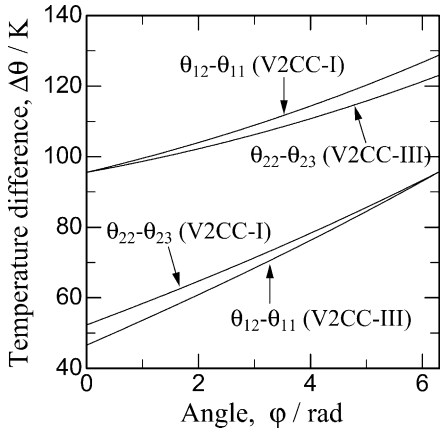

Fig. 7. Temperature difference between the cylinder surfaces of V2CC systems, when the output power becomes the maximum.

4.6. Mode I and III

The output powers of Mode I and II were always larger than those of III and IV, as shown in Fig. 4. This reason can be found in the length of fluid path as discussed below. Here, V2CC-I and V2CC-III systems are picked up as the example.

The temperature drop of the hot fluid was nearly the same both in two systems as shown in Fig. 5. However, the temperature rises of the coolant were different. The surface temperature differences $\Delta\theta$ were shown in Fig. 7. $\Delta\theta$ of V2CC-I system were always larger than $\Delta\theta$ of V2CC-III. It is explained by the difference of fluid path length, $2\pi r$, at the outer and inner paths. Because the cold fluid at V2CC-III system is warmed during the first circulation in the longer outer path, T_3(V2CC-III, $\varphi = 2\pi$) becomes higher than T_1(V2CC-I, $\varphi = 2\pi$). The fluid after the first circulation with this higher temperature of V2CC-III system enters into the inner path for the second circulation. Then the $\Delta\theta$ of the inner cylinder becomes smaller. As deduced in Eq. (7), the summation of $\Delta\theta$ is proportional to E. Therefore, V2CC-I system can generate larger E than V2CC-III system. Note that $r_{11}^{opt.}$(V2CC-I) is nearly equal to $r_{11}^{opt.}$(V2CC-III), and the internal electric resistance of power plant is the same. We may conclude, therefore, that the larger temperature difference of the fluids should be given at the surface of the inner thermoelectric cylinder for higher P.

4.7. Effects of panel thickness and path width

The thicker thermoelectric cylinder can keep the hot fluid temperature high, because the heat exchange through the cylinder delays. Therefore, the higher output power is expected when the thermoelectric cylinder becomes thicker. Using the analytical expression of the output power

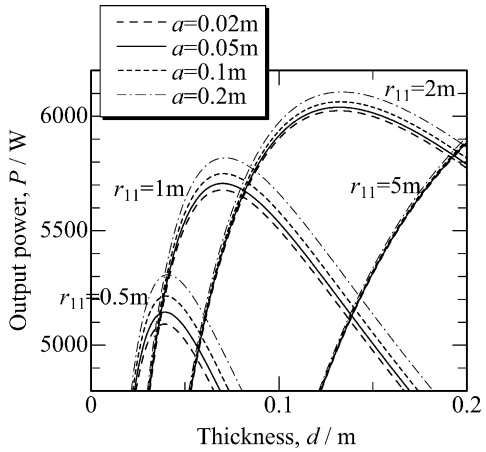

Fig. 8. Optimum thickness for the maximum output power in V2CC-I system, where the cylinder length $w = 2$ m. r_{11} and a are the inner radius of the inner cylinder and the fluid path height, respectively.

from V2CC-I system (Table 2) as a model, the effect of the panel thickness, d, on P(V2CC-I) was calculated in Fig. 8.

When the inner radius of the cylinder, r_{11}, was fixed, P has the maximum at an optimum thickness. The decrease of P at the thicker panel was due to the larger electric resistance. This maximum of P, P^{max}, became larger as r_{11} increased. Simultaneously the optimum thickness for P^{max} increased. This is due to the smaller drop of temperature difference between two fluids when the heat exchange becomes the less.

The path height of the fluid, or the gap distance between the cylinders, a, did not change P seriously. a and d did not affect the optimum radius, $r_{11}^{opt.}$. However, it is noted that this work used a constant heat transfer coefficient, h. Practically, h depends on the mass flow rate and the cross-section of the path [11,12]. Therefore, the influence of a will be studied further.

5. Conclusion

This work studied the thermoelectric power generation with cylindrical double tubes in which thermoelectric elements were embedded. The fluid path connections were designed as the roll-cake. Sixteen kinds of the system design were analyzed using the steady heat balance, and their output powers P were expressed in eight mathematics equations. The V2CC-I and V2CC-II system were chosen by the largest output power P^{max} at the optimum radius. Their two cylinders were exposed to the two counter flows. Because the temperature difference of two fluids can be kept larger after the first circulation, the fresh fluids should enter from the inside of the inner cylinder (Mode I and II). V2CP and V2PC systems may cause the larger pressure loss, and V2PP systems did not show the large P^{max}. V2CC-I and V2CC-II system can generate the equivalent power to V1C systems, using only 36% material of V1C.

Acknowledgements

The author thanks to Mr. Hiroshi Hattori for his assistance, and Mr. Shin-ichi Toda for his useful discussions. This work was supported in part by Japan Nuclear Cycle Development Institute (JNC), Yazaki Memorial Foundation for Science and Technology, and Sekisui Chemical Co. Ltd.

References

[1] K. Ono, R.O. Suzuki, R. Nakahashi, M. Shoda, Tetsu-to-Hagané 83 (2) (1997) 157–161.
[2] K. Ono, R.O. Suzuki, Proceedings of the 17th International Conference on Thermoelectrics, IEEE, Piscataway, NJ, 1998, pp. 515–518.
[3] K. Ono, R.O. Suzuki, J. Met. December (1998) 49–51.
[4] B. Mathiprakasam, T. Sutikno, J. Beeson, Proceedings of the 4th International Conference on Thermoelectrics, IEEE, Piscataway, NJ, 1982, p. 61.
[5] J. Esarte, G. Min, D.M. Rowe, J. Power Sources 93 (2001) 72–76.
[6] T. Kyono, R.O. Suzuki, K. Ono, IEEE Trans. Energy Conversion 18 (2) (2003) 330–334.
[7] R.O. Suzuki, D. Tanaka, J. Power Sources 122 (2) (2003) 201–209.
[8] R.O. Suzuki, D. Tanaka, S. Toda, Proceedings of the 22nd International Conference on Thermoelectrics, IEEE, Piscataway, NJ, 2003, in press.
[9] R.O. Suzuki, D. Tanaka, J. Power Sources 124 (1) (2003) 293–298.
[10] R.O. Suzuki, D. Tanaka, J. Power Sources, 2003, in press.
[11] S. Isshiki, N. Kitayama, Technology of Heat Transfer, Morikita Press, Tokyo, 1984.
[12] W.M. Kays, M.E. Crawford, Convective Heat and Mass Transfer, second ed., McGraw-Hill, New York, 1980.
[13] R. Sakata (Ed.), Thermoelectrics, Principles and Applications, Realize Inc., Tokyo, 2001.